Bilayer Thin Films That Combine Luminescent and Spin Crossover Properties for an Efficient and Reversible Fluorescence Switching

Alin-Ciprian Bas, Xavier Thompson, Lionel Salmon, Christophe Thibault,
Gábor Molnár, Oleg Palamarciuc, Lucie Routaboul, Azzedine Bousseksou

Article

Bilayer Thin Films That Combine Luminescent and Spin Crossover Properties for an Efficient and Reversible Fluorescence Switching

Alin-Ciprian Bas [1,2], **Xavier Thompson** [1], **Lionel Salmon** [1], **Christophe Thibault** [2], **Gábor Molnár** [1], **Oleg Palamarciuc** [3,4], **Lucie Routaboul** [1,*] **and Azzedine Bousseksou** [1,*]

1   LCC-CNRS, Université de Toulouse, CNRS, 31077 Toulouse, France; alinciprian.bas@gmail.com (A.-C.B.); xavier.thompson95@gmail.com (X.T.); lionel.salmon@lcc-toulouse.fr (L.S.); gabor.molnar@lcc-toulouse.fr (G.M.)
2   LAAS-CNRS, Université de Toulouse, CNRS, 31077 Toulouse, France; cthibaul@laas.fr
3   Department of Chemistry, Moldova State University, MD-2009 Chisinau, Moldova; palamarciuco@gmail.com
4   Polivalent-95 SRL, MD-2028 Chisinau, Moldova
*   Correspondence: lucie.routaboul@lcc-toulouse.fr (L.R.); azzedine.bousseksou@lcc-toulouse.fr (A.B.)

![check for updates]

Abstract: We report on the vacuum thermal deposition of bilayer thin films of the luminescent complex Ir(ppy)$_3$, tris[2-phenylpyridinato-C2,N]iridium(III), and the spin crossover complex [Fe(HB(tz)$_3$)$_2$], bis[hydrotris(1,2,4-triazol-1-yl)borate]iron(II). Switching the spin state of iron ions from the low spin to the high spin state around 337 K leads to a reversible jump of the luminescence intensity, while the spectrum shape and the luminescence lifetime remain unchanged. The luminescence modulation occurs due to the different UV light absorption properties of the iron complex in the two spin states and its magnitude can therefore be precisely adjusted by varying the film thickness. These multilayer luminescence switches hold potential for micro- and nanoscale thermal sensing and imaging applications.

Keywords: spin crossover; luminescence; thin films

1. Introduction

Fluorescence switches are systems, which contain a light-emitting fragment whose emission can be quenched reversibly through an external parameter [1]. Fluorescence switches are very useful notably for detection, imaging and optical storage devices. Therefore, they have applications in a large range of fields, from health to informatics via environment [2–5]. The concept of fluorescence switches requires a way to controllably and reversibly modify the luminescence intensity. To obtain a modification of the luminescence activity, an external stimulus (chemical, thermal, mechanical, etc.) is applied to the system [6–9].

In this context of luminescence switching, an attractive strategy consists of fabricating a hybrid material, which combines a luminophore species with a spin crossover (SCO) molecule. The latter are transition metal complexes, which can be reversibly switched between the low spin (LS) and the high spin (HS) states of the central metal ion [10–13]. The SCO is trigged by the application of an external stimulus, such as an increase or decrease of pressure or temperature, light irradiation (LIESST effect [14]), or the presence of an intense magnetic field [15]. The SCO phenomenon leads to a significant change in the chemical and physical properties of the metal complex including the modification of its magnetic susceptibility, dielectric permittivity, mass density, color, refractive index, and elastic moduli. SCO complexes have recently received increasing interest because they offer an opportunity to fabricate switchable nanomaterials and devices [16,17]. When combined with a luminophore, the presence

of the SCO complex permits the transformation of a stimulus which has no (or moderate) effect on the luminescent property, into a stimulus, which strongly influences the emission intensity [18]. For example, the luminescence intensity in general slowly decreases at increasing temperatures due to the thermal activation of non-radiative decay channels [19]. However, this trend can be inversed by associating the luminophore to an SCO complex, which will strongly quench the luminescence in the low temperature (LS) state.

The combination of a luminophore with a SCO complex can lead to a luminescence modulation fundamentally by three different pathways: (i) the luminescence emission can be selectively re-absorbed by either the HS or the LS state, depending on the overlap between the emission spectrum of the luminophore and the absorbance of the complex in a given spin state. This will lead to a modulation of the luminescence intensity and, in certain cases, to spectral shifts, but the excited state lifetime of the luminophore will remain obviously unaffected. For example, this 'emission—reabsorption' mechanism has been proposed to be dominant in refs [20,21]. (ii) Alternatively, the excited state energy of the luminescent molecule can be transferred to the metal complex via Förster-type dipole–dipole interactions [19] without photon emission. Since this resonant process is also governed to a large extent by the spectral overlap between the complex and the luminophore, it will occur selectively in one or the other spin state. Consequently, the luminescence emission intensity can be drastically quenched, but in contrast to the re-absorption scenario, this will be also accompanied by the modulation of the luminescence lifetime. On the other hand, no significant spectral shifts are expected for such energy transfer process. To our best knowledge, there is no literature report wherein this mechanism could be unambiguously demonstrated for a luminescent SCO material. (iii) Finally, various 'environmental effects' may also lead to the modulation of the luminescence upon the SCO process [19]. These effects include the change of the polarity and stiffness of the local environment, the modulation of intermolecular distances as well as charge transfer phenomena. Contrary to the re-absorption and energy transfer phenomena, the occurrence and manifestation of this last category of effects remains difficult to predict and interpret. The change of local environment involves in most cases not only the modulation of emission intensity, but also a change of the non-radiative decay rate and spectral shifts. The most obvious diagnostic feature of these phenomena remains, however, the feeble correlation between the luminescence modulation and the spectral overlaps. We believe that these 'environmental effects' play a non-negligible role in most reported examples of luminescent SCO materials.

Previous literature, which associate SCO and luminescent properties in a hybrid material, reports classification according to four categories [18]. (i) In the first case, the SCO complex contains a luminescent ligand [22–36]. Albeit elegant, one main challenge of this 'luminescent-SCO complex' strategy is the possibility to lose the SCO and/or the luminescent properties, which remain rather difficult to predict for a rational design of new complexes. In addition, the high concentration of luminophores may lead to self-quenching. (ii) The second strategy consists of mixing (doping) the SCO material with a fluorophore [21,37–41]. This can usually be achieved in a straightforward manner by adding a few percent of luminescent species to the SCO material during the synthesis of the latter. The advantage of this approach is its simplicity and efficiency. However, it is often difficult to control the homogeneity of the material and to locate the luminophore within the mixture. (iii) To overcome the latter problem one might also partially substitute different components of the SCO material (e.g., the counter-ions, the ligands or even the metal ion) by a chemically similar, but luminescent species. This way one may obtain 'co-crystals' of the SCO and the luminescent species [42–44]. This 'substitution approach' can be seen also as a combination of the first two strategies. Yet, it is still not guaranteed that the substituted material will conserve intact the properties of each constituent. Indeed, the introduction of the luminescent molecule into the SCO material, even in low percentage, can lead to a significant change of the SCO properties and, vice-versa, the luminescence may also be drastically altered by the SCO crystal lattice. (iv) In a fourth strategy, the luminophore and the SCO parts are juxtaposed in a spatially controlled assembly [45–50]. This strategy was mainly applied to the synthesis of nanoparticles with a SCO core and a luminescent shell. Notably, $[Fe(Htrz)_2(trz)]BF_4$ (trz = triazolato)

SCO nanoparticles were covered by a thin silica layer and luminescent molecules were then grafted on the oxide surface [46]. This way the luminophores are well localized, while they are not expected to interfere substantially with the SCO properties of the core-shell particles.

In this article, we present a novel approach for luminescence modulation by SCO, based on bilayer film deposition, which is conceptually similar to the last strategy of 'spatially controlled assembly'. Indeed, SCO thin films have recently received much attention for their possible technological applications [16,17]. In a few cases, SCO thin films were even endowed with luminescent properties [38–40]. Yet, the mechanism of the luminescence switching is completely new in the present work: we use the SCO film as a switchable UV filter to modulate the excitation light intensity. We show that by an appropriate combination of materials their properties can be preserved by this straightforward approach and it becomes therefore possible to modulate, in a fully reversible and predictable manner, the emission intensity of a luminescent film using a thin, transparent SCO top-coating.
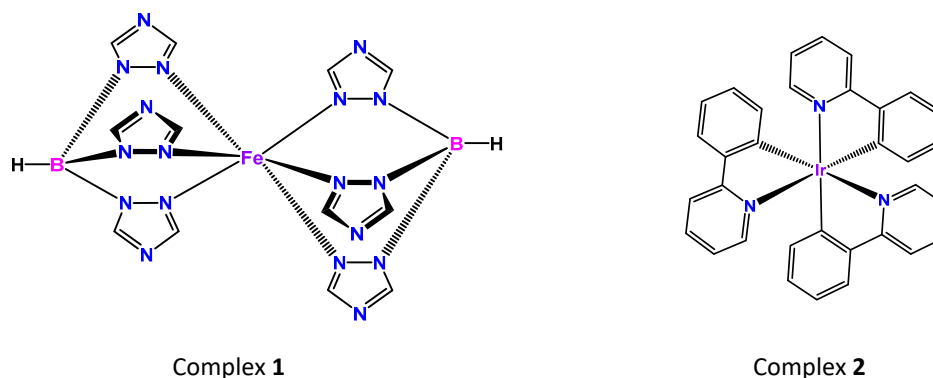
2. Experimental Section

Reagents and solvents used in this study are commercially available. The bulk powder of [Fe(HB(tz)$_3$)$_2$] was synthesized as described in Reference [51]. The Ir(ppy)$_3$ powder was obtained from Sigma Aldrich and used without any further purification. The fused silica substrates were purchased from SCHOTT AG and cleaned with acetone and 2-propanol to remove contaminants. Multilayer films were grown by thermal evaporation in a PREVAC thermal deposition system at a base pressure of ca. 2×10^{-7} mbar. The SCO (luminescent) complex was heated until 250 °C (280 °C) in a quartz crucible and evaporated at a rate of 0.07 Å s^{-1} (0.03 Å s^{-1}). For co-deposition, the two complexes were evaporated simultaneously at a pressure of ca. 5×10^{-7} mbar. The deposition rate was 0.2 Å s^{-1} and 0.03 Å s^{-1} for the [Fe(HB(tz)$_3$)$_2$] and Ir(ppy)$_3$ molecules, respectively. After deposition, the [Fe(HB(tz)$_3$)$_2$] films were annealed for 10 min at room temperature in ca. 80% relative humidity air in order to achieve a better crystallinity. The evaporation rate and film thickness were monitored in situ using a quartz crystal microbalance. The final determination of the film thickness and topography was carried out using a Cypher ES atomic force microscope (AFM) from Oxford Instruments in amplitude modulation mode in ambient air using OMCLAC160TS-R3 (Olympus, Tokyo, Japan) probes.

Grazing incidence X-ray diffraction (GIXRD) experiments were carried out in a PANalytical X'Pert PRO MPD system using Cu-Kα radiation (45 kV and 40 mA) with a parallel-beam configuration. The incident beam optics consisted of a mirror with a 1/32° divergence slit. A parallel plate collimator (0.18°) and Soller slits (0.04°) were mounted on the path of the diffracted beam. An X'Celerator detector in receiving slit mode was used for X-ray collection. Temperature-dependent absorbance spectra of the films were collected at wavelengths between 200 and 800 nm using a Cary 50 (Agilent Technologies, Santa Clara, CA, USA) spectrophotometer and a Linkam FTIR-600 heating/cooling stage (equipped with fused silica windows). The sample chamber was purged by dry nitrogen and spectra were acquired in the 293–393 K range with 1 K/min scan rate. A Fluoromax-4 (Horiba, Tokyo, Japan) spectrofluorimeter equipped with a xenon lamp source and an Optistat DN-V liquid nitrogen cryostat connected to an ITC601 temperature controller (Oxford Instruments, Abingdon-on-Thames, UK) was used to acquire fluorescence excitation and emission spectra as a function of temperature. Fluorescence spectra were corrected for the instrumental response as implemented in the software. Luminescence lifetime measurements were performed using the time-correlated single photon counting (TCSPC) technique by means of a DeltaFlex (Horiba, Tokyo, Japan) instrument equipped with a 303 nm (pulse duration ~1 ns) as well as with a 280 nm (pulse duration > 100 ns) electroluminescent diode. Variable temperature lifetime measurements were conducted using the Optistat DN-V cryostat. Fittings and lifetime calculations were performed using DAS6 fluorescence decay analysis software (Horiba, Tokyo, Japan).
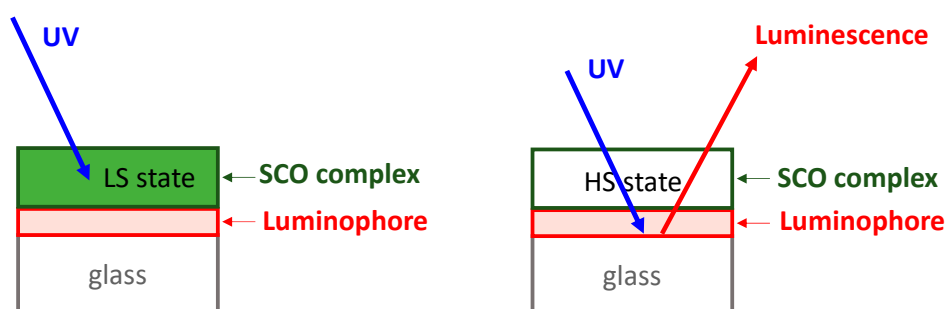
3. Results and Discussion

On a transparent substrate, we aim to stack a thin layer of luminescent molecules covered by a layer of SCO molecules in order to achieve a luminescence intensity modulation driven by the spin state switching phenomenon. Obviously, the choice of the two types of molecules is crucial. We decided to combine the bis[hydrotris(1,2,4-triazol-1-yl)borate]iron(II) SCO compound ([Fe(HB(tz)$_3$)$_2$] complex **1**) with the tris[2-phenylpyridinato-C2,N]iridium(III) luminophore ((Ir(PPy)$_3$)-complex **2**) (Scheme 1).

Complex **1**   Complex **2**

Scheme 1. Chemical structure of the iron and iridium complexes.

Recently, we have carried out a deep investigation of the SCO complex **1** in different forms (single crystal, powder and thin film) and it appears to us as an excellent candidate to perform this study [51–58]. Indeed, this compound is a rare example of sublimable spin crossover complexes (globally neutral with low molecular weight), therefore SCO films of complex **1** can be prepared by vacuum evaporation on a substrate. In these films, the SCO phenomenon is similar to the one observed in the solid state: they display a full and abrupt transition around 337 K (64 °C) with a narrow hysteresis loop of ca. 1 K width. These films can potentially be used for optical applications since sub-micrometric layers of **1** are transparent in the visible and near-infrared spectral ranges in both spin states. In addition, when using an appropriate annealing procedure they form a homogenous nano-crystalline texture with smooth surface topography, hence not only absorption, but also scattering losses are very small. On the other hand, complex **1** in the LS state absorbs much more UV light than in the HS state. For example, at 318 nm the absorption coefficient (3×10^4 cm^{-1}), related most probably to a singlet-singlet charge transfer transition between the metal center and the ligand, vanishes completely when switching the complex from the LS (^{1}A) to the HS (^{5}T) state. It is this huge optical density change that we would like take advantage of in modulating the intensity of the luminescence. Indeed, complex **1** in the LS state will strongly absorb and thus block UV irradiation. Whereas, in the HS state, it is quasi-transparent in the UV, so the main part of the irradiation will reach and excite the luminophore layer underneath (Scheme 2). Therefore, we expect that the luminescent intensity of the material with complex **1** in the LS state should be substantially weaker than with **1** in HS state. Obviously, this strategy implies that UV irradiation should be used to excite the luminescence emission. To this aim we have chosen the luminescent complex Ir(PPy)$_3$, which is probably one of the most studied molecules in the Organic Light-Emitting Diode (OLED) field and deep investigations have been performed in order to understand its luminescent properties [59–62]. This compound is well known to absorb light in the UV between 250 and 320 nm, which has been assigned to singlet-singlet π-π* transitions of the ligand [62]. It is well documented that its excitation under UV irradiation leads to a prominent green emission centered at 515 nm, which is attributed to the radiative decay of the triplet ^{3}MLCT (metal ligand charge transfer) state to the ground state [62]. As the SCO film is transparent in visible region, this green emission of complex **2** will not significantly be attenuated by the presence of a thin layer of complex **1**. Besides these favorable and very well documented luminescent properties, we

shall note that compound **2** is easily available commercially and can be prepared in thin film form by vacuum evaporation.

Scheme 2. Outline of the bilayer stack and the spin state dependent UV filter mechanism.

Films of complex **2** were made by thermal evaporation under high vacuum. Optical microscopy and atomic force microscopy (AFM) observations revealed the formation of homogeneous films (Figure 1a,b). From the AFM measurements, a film thickness of ca. 30 nm and the root-mean-square (RMS) surface roughness of ca. 0.3 nm was inferred. Interestingly, the obtained film morphology is rather different from the rod-like structures previously reported in the literature [62]. However, GIXRD measurements indicate that, contrary to those reports, the films of **2** made by us are amorphous (see Figure 1c), which is probably the main reason for the different film morphologies.

Figure 1d represents the UV-vis absorbance spectrum of the film of **2** on a fused silica substrate. We observe absorbance bands around 300 nm and 400 nm (note that strong absorption below ca. 250 nm occurs due to the substrate). The excitation of the film in these absorption bands yields a broad luminescent emission centered at 520 nm (Figure 1e). The temperature dependence of this luminescence intensity turned out to be negligible in the investigated range (from 300 K to 370 K, see inset of Figure 1e).

This property is very advantageous as it allows one to investigate the influence of the thermal SCO phenomenon without any intricacy due to intrinsic luminescence thermal quenching phenomena. In a similar fashion, it appears that the luminescent lifetime of films of **2** is not temperature dependent either (see Figure 1f). The luminescence decay can be reasonably well fitted only with three exponential functions from which the average lifetime is estimated to be 3 µs, which is consistent with previous literature reports [61,62].

In the next step, a 107 nm thick film of the SCO complex **1** was deposited by vacuum thermal evaporation on top of the luminophore layer. Optical microscopy and AFM images (Figure 2a,b), clearly show the change of surface morphology and reveal the formation of some islands. The RMS surface roughness of the bilayer is around 3 nm (for a bilayer thickness of 30 + 107 nm), which is higher than typical values obtained after the evaporation of the SCO complex directly on the fused silica substrate. Figure 2c shows a typical GIXRD trace for a bilayer film evidencing a single diffraction peak near $2\theta = 10°$. In line with our previous investigations [53], this diffraction pattern denotes that the films of **1** deposited on top of the fluorescent layer are crystalline and oriented.

Figure 2d represents the absorbance spectra of the bilayer acquired at different temperatures between 293 and 393 K. As expected, the low temperature (i.e., low spin) absorbance spectrum overlaps with that of the iridium complex around 300 nm. When heating the sample above the spin transition temperature the optical density of the SCO film decreases drastically. For example, at 300 nm the absorbance of the bilayer drops by $\Delta_{abs} = 0.33$ when going from the LS to the HS state. The highest absorbance change ($\Delta_{abs} = 0.39$) is observed at 318 nm, which corresponds to our previous observations for a complete spin transition in film of **1** with ca. 120 nm thickness. The absorbance change as a function of temperature at this wavelength is shown in Figure 3. An abrupt and well reversible change of the absorbance occurs around 337 K with a small hysteresis. This thermal spin transition curve is virtually the same as it was observed for films deposited directly on glass substrates, from which

we can infer that the SCO properties of complex **1** are not significantly modified by the presence of the luminescent film underneath. This result corroborates our previous observations [53] about the negligible role of the nature of the substrate on the properties of films of **1**. Figure 2e depicts the luminescence emission spectra of the bilayer film at different temperatures. Overall, these spectra closely resemble that of the neat fluorescent film, despite the excimer shoulder around 600 nm which is somewhat more intense. Remarkably, in the bilayer, the luminescence intensity changes drastically between ca. 333 and 350 K, in harsh contrast with the quasi-constant luminescent intensity of the film of complex **2** in the same temperature range. On the other hand, the luminescent lifetime of **2** is not significantly altered by the presence of the SCO layer and the decay curves remain virtually temperature independent (Figure 2f).
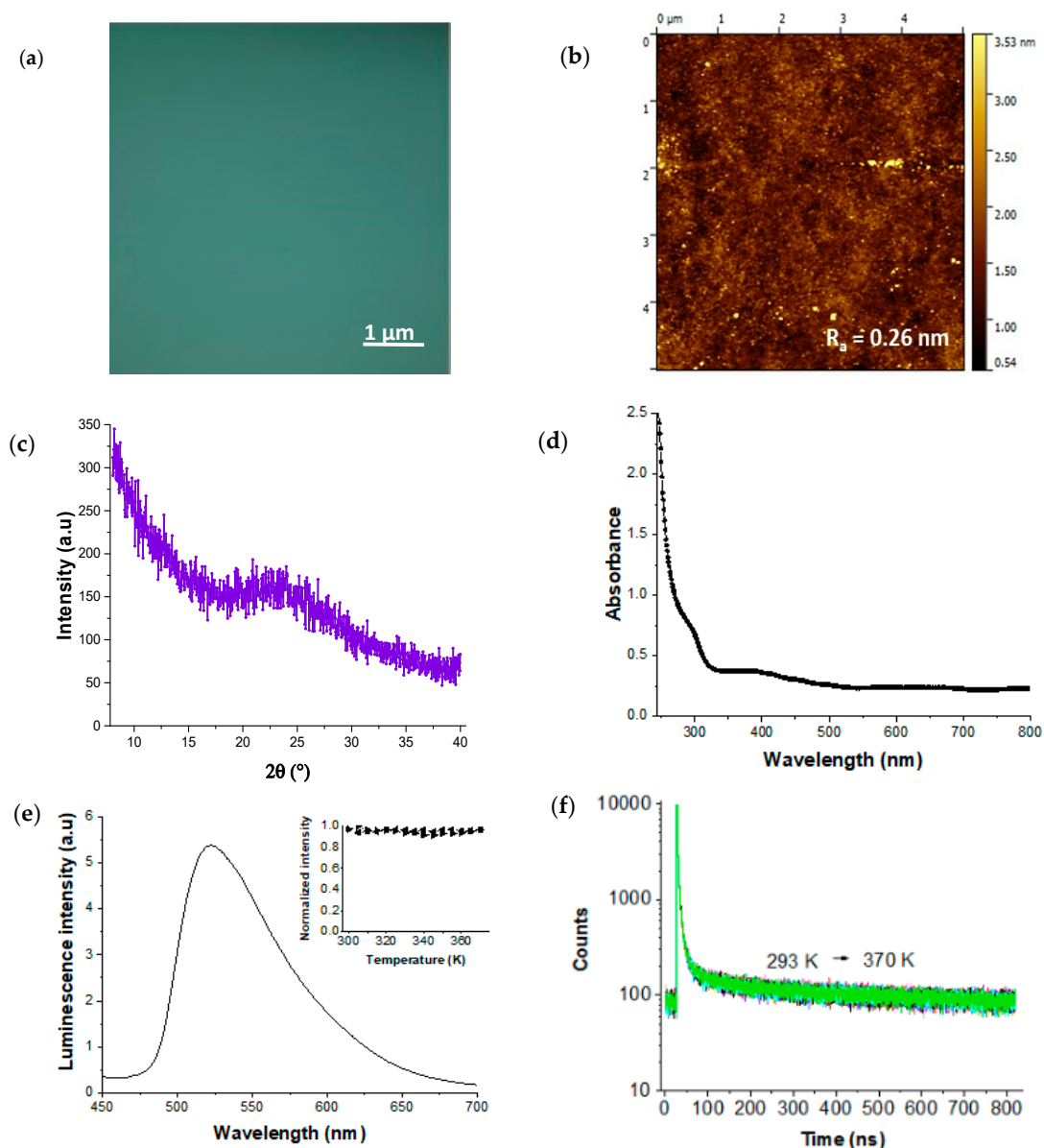

Figure 1. Characterization of films of Ir(PPy)$_3$. Typical optical microscopy (**a**) and AFM topography (**b**) images, (**c**) GIXRD pattern, (**d**) UV-vis absorption spectrum, (**e**) luminescence emission spectrum (excitation: 300 nm, high pass filter $\lambda_{emission}$ > 400 nm) and its temperature dependence in insert and (**f**) variable temperature luminescent decay curves (excitation: 303 nm, emission 520 nm) recorded over the first 800 ns of the decay.
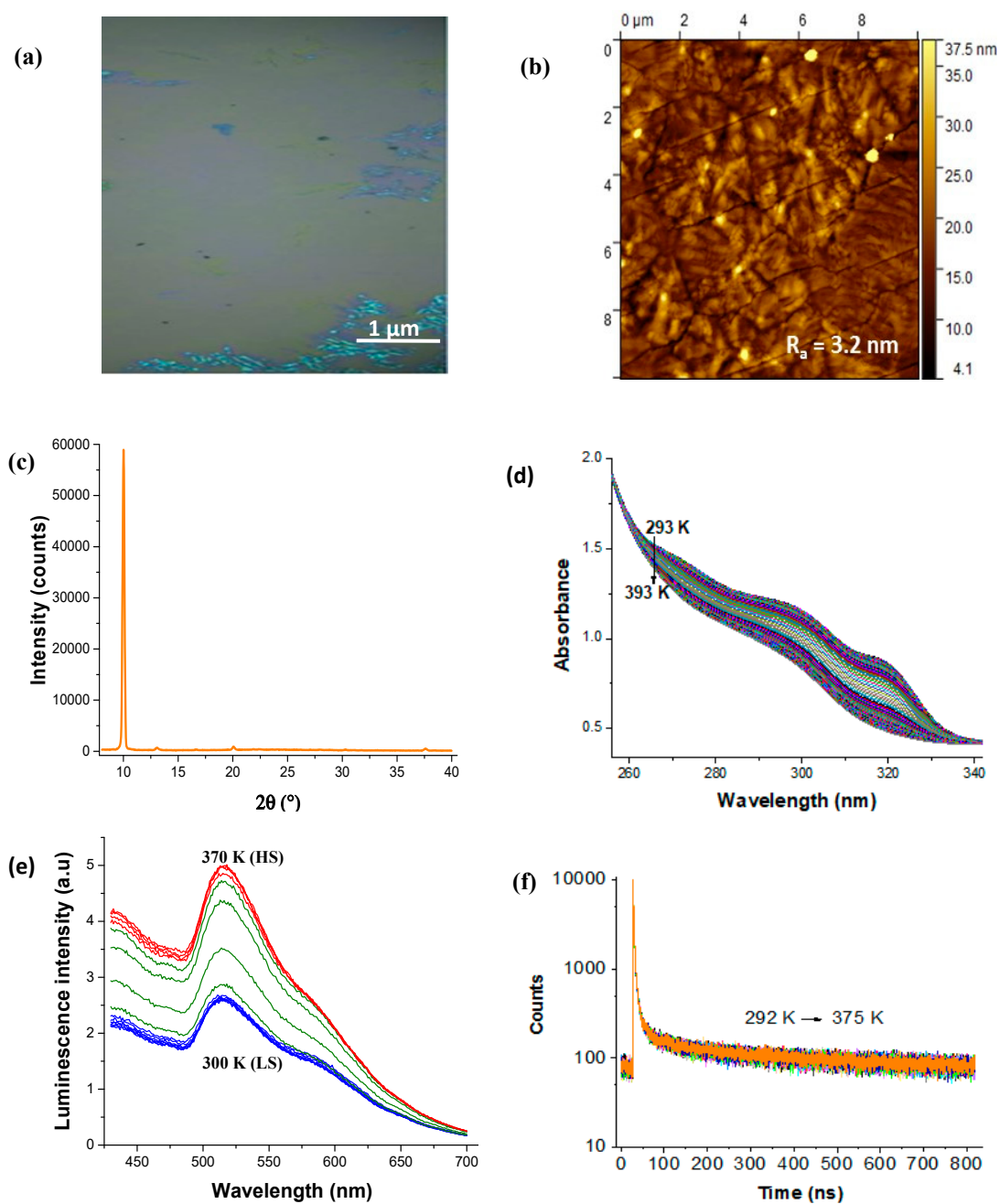
Figure 2. Characterization of bilayer films of Ir(PPy)$_3$ and [Fe(HB(tz)$_3$)$_2$]. Typical optical microscopy (**a**) and AFM topography (**b**) images, (**c**) GIXRD pattern, (**d**) variable temperature UV absorption spectra, (**e**) variable temperature luminescence emission spectra (excitation: 300 nm, high pass filter $\lambda_{emission}$ > 400 nm) and (**f**) variable temperature luminescence decay curves (excitation: 303 nm, emission 520 nm) recorded over the first 800 ns of the decay.
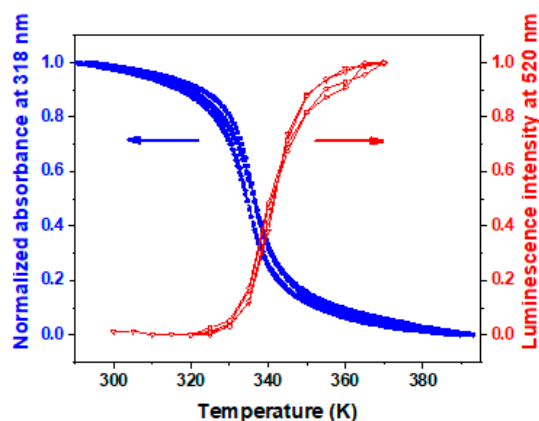
Figure 3. Luminescence modulation: Normalized temperature dependence (over two heating-cooling cycles) of the UV absorbance (318 nm) and of the luminescence intensity (excitation: 300 nm, emission 520 nm) for a bilayer film of 30 + 107 nm thickness.

In Figure 3 we compare the temperature dependences of the absorbance (λ = 318 nm) and the luminescence intensity ($\lambda_{excitation}$ = 300 nm, $\lambda_{emission}$ = 520 nm) for the bilayer film over two thermal cycles between 300 and 380 K. The drastic increase in the intensity of the luminescence above ca. 335 K can be unambiguously attributed to the spin transition phenomena (note that the slight difference in SCO temperatures observed in absorbance and fluorescence experiments can be attributed to the different heating-cooling equipment used to control the temperature of the sample). It may be worth to note also the good overall reproducibility of these measurements over successive heating-cooling cycles, despite a small, continuous decrease of the luminescence intensity due to a slow (hours scale) photo-bleaching phenomena.

At this point, we can conclude that the intrinsic properties of each compound, luminescent and SCO, are not significantly affected by the presence of each other. Yet, we observe a reversible modulation of the luminescence intensity at the SCO, which we can attribute to the different UV absorbance properties of the iron complex in its two different spin states: either fully transmitting (HS state) or partially blocking (LS state) the light beam used for luminescence excitation. This hypothesis is supported by the fact the promotion of the iron complex from the LS to the HS state doubles the luminescence intensity of our bilayer film, while its UV transmittance (λ = 300 nm) doubles as well. In the same time, the luminescence spectral shape and lifetime remain temperature and spin-state independent, which is also fully compatible with the proposed mechanism.

In order to obtain further proof for this explanation and to verify the scalability of the luminescence modulation amplitude, we have prepared two other bilayer samples with SCO layers of ca. 200 nm and 800 nm thickness. For the thickest sample, we had to overcome a difficulty concerning the formation of crystalline films. As mentioned above, oriented, crystalline SCO films of **1** are obtained by annealing the pristine evaporated film in humid air with ca. 80% relative humidity. However, this method is not fully efficient when the thickness of the film is greater than ca. 200 nm. To prepare the sample with 800 nm of SCO thickness, we have therefore first deposited an SCO layer of 200 nm on top of a 30 nm layer of **2** and we have annealed the film as usual. Then, we have put back the annealed sample in the evaporator to grow an additional 600 nm thick layer of SCO molecules. Post deposition AFM measurements agree with the value indicated by the quartz balance and confirm that the thickness of the SCO layer is around 800 nm. X-ray diffraction on this thick film revealed only one significant diffraction peak near 2θ = 10° indicating crystallinity and preferred orientation. However, the XRD intensity and the UV absorbance of this film correspond to a film thickness of only ca. 500 nm. The significant difference between the film thickness values of AFM/quartz balance (~800 nm) and XRD/UV-absorbance (~500 nm) can be explained by a formation of an SCO film with a partial crystallinity and thus partial spin transition.

The results obtained with the three different SCO film thickness are summarized in Figure 4. The spin transition curves are comparable for each sample in terms of spin transition temperatures, though slight differences in the shape of the curves can be depicted (Figure 4a).
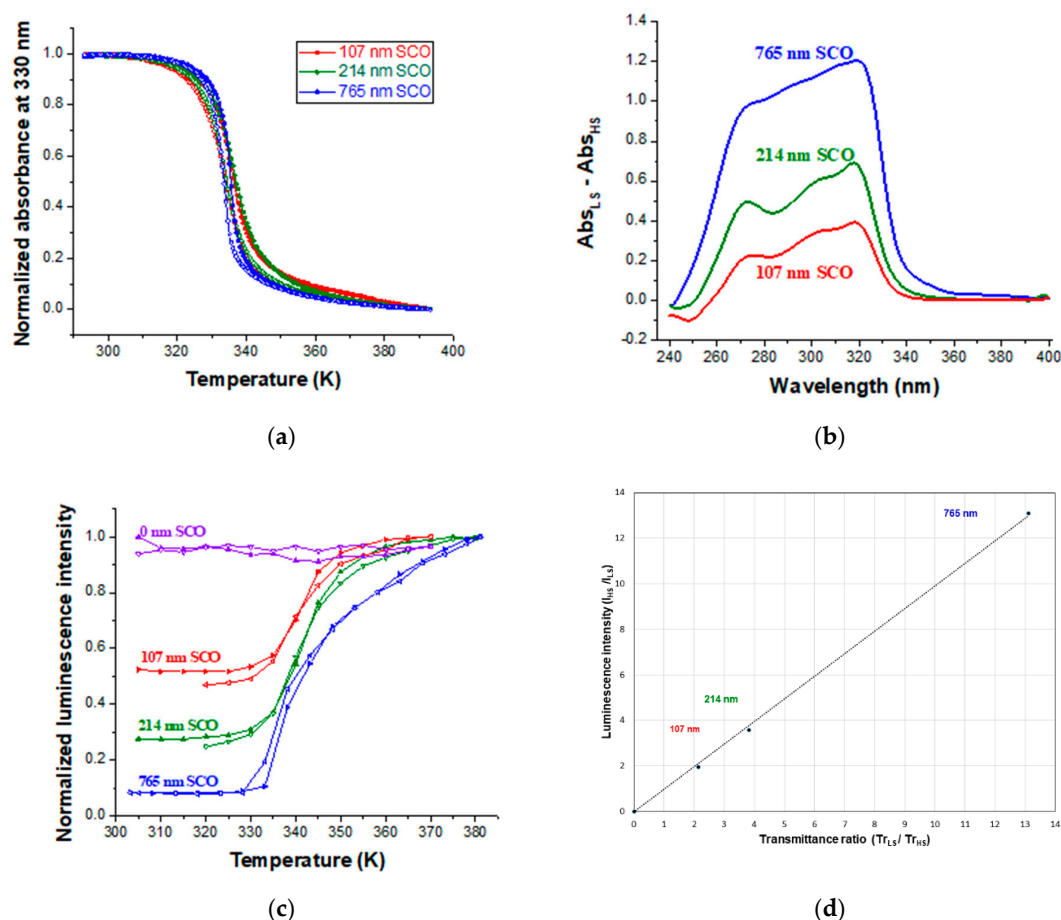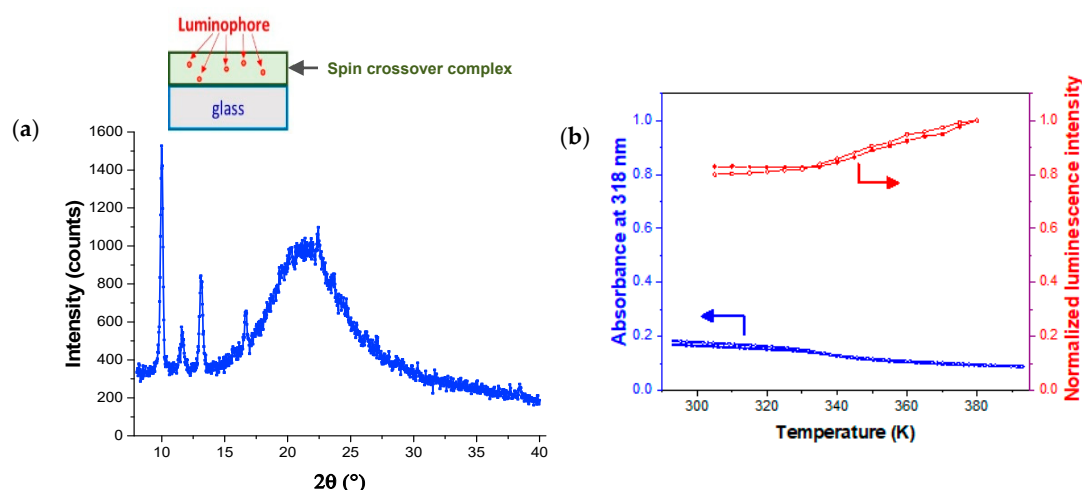

Figure 4. Correlation between the absorbance of $[Fe(HB(tz)_3)_2]$ and the luminescence of $Ir(PPy)_3$. (**a**) Normalized temperature dependence of the UV absorbance (at 330 nm) for three bilayer samples with different SCO layer thicknesses (107, 214 and 765 nm). (**b**) Absorbance changes associated with the SCO for different SCO film thickness. (**c**) Normalized temperature dependence of the luminescence intensity for different SCO film thickness. (**d**) Plot of the luminescence intensity ratio vs. the UV transmittance ratio between the HS and LS states. The corresponding SCO film thickness is also shown.

In response to the absorbance change between the LS and HS states (ΔA_{LH}) (Figure 4b), an important and reversible change of the luminescence intensity is also observed around 337 K (Figure 4c) in each bilayer sample. As expected, the extent of the luminescence modulation (I_{HS}/I_{LS}) increases with the thickness of the SCO layer. Changes from ca. 200% to 1300% (with reference to the room temperature value) from the thinnest to the thickest film are obtained (see Table 1). The most remarkable point, as illustrated both in Table 1 and Figure 4d, is the perfect one-to-one correlation between the luminescence modulation I_{HS}/I_{LS} in the film of **2** and the transmittance change Tr_{HS}/Tr_{LS} in the film of **1**. In other words, the UV transmittance of the SCO films gives an accurate scale of modification of the luminescence intensity of the Ir complex. This means that one can modulate the luminescence intensity 'at will' by adjusting the thickness of the SCO layer. The results in Figure 4 provide irrefutable proof of the mechanism of luminescence modulation in the bottom layer, which occurs via the modulation of the exciting light intensity by the spin-state dependent UV absorbance of the top layer. (It may be worth to note that by changing the thickness of the luminescent layer, we possibly change the ratio of monomer/excimer emissions, which may alter the SCO modulation amplitude.)

Table 1. Comparison of the UV absorption and luminescent properties of bilayer films with different thickness of SCO layers.

Thickness of SCO Layer	$\Delta_{Abs} = Abs_{LS} - Abs_{HS}$		Tr_{max}/Tr_{min} at 300 nm	I_{max}/I_{min}
	At 300 nm	**At 318 nm**		
107 nm	0.331	0.392	2.14	1.95
214 nm	0.582	0.755	3.82	3.59
765 nm	1.118	1.204	13.05	13.12

We have also investigated if a closer contact between the SCO and luminescent molecules in a mixed film could allow for an efficient luminescence modulation. Indeed, a few examples in the literature demonstrate that a luminescent molecule can interact strongly and selectively with SCO complexes in either the low or the high spin state [18]. Obviously, the probability of an efficient electronic energy transfer between the triplet emitting state of the luminophore and the week singlet d-d absorption band of the LS complex is extremely low. Nevertheless, one might expect a significant amplification or quenching of the luminescence emission via 'environmental effects' related to the structural changes which accompany the SCO. In any case (i.e., electronic or structural effects), a close proximity between the two types of molecules is required. To investigate this possibility we co-evaporated the SCO and luminescent molecules to form mixed films with ca. 12%, 15% and 21% nominal luminophore content. Overall, we observed that for increasing doping levels the SCO properties of the films degrade and the luminescence modulation thus becomes negligible. Figure 5 summarizes the results obtained for the lowest doping (12%). As shown in Figure 5a, the X-ray diffraction spectrum of the doped film can be ascribed to an amorphous/semi-crystalline film without any particular texture. This means that the presence of the luminophore molecules within the deposit inhibit the recrystallization of the SCO film. Consequently, the spin transition curves obtained from variable temperature absorbance measurements on the mixed films (Figure 5b) are very different from what we generally observe for the pure films of **1**. In particular, the absorbance change associated with the SCO is very low ($\Delta A = 0.057$); it is approximately ten times smaller than what is expected for a pure SCO film with the same thickness. As it can be expected, we observe thus only a very weak effect of the spin transition on the luminescence emission intensity ratio ($I_{HS}/I_{LS} = 1.2$) (Figure 5b).

Figure 5. Characterization of a [Fe(HB(tz)$_3$)$_2$] film doped with 12% Ir(PPy)$_3$. (**a**) Representative GIXRD pattern. The inset shows the outline of the sample. (**b**) Temperature dependence of the UV absorbance (318 nm) and of the luminescence intensity (excitation: 300 nm, emission 520 nm) on heating and cooling.

4. Conclusions

In this manuscript, we outlined an efficient approach to fabricate hybrid materials, which combine luminescent and spin crossover molecules in a bilayer film stack. Crucially, we have shown that the intrinsic properties of the two layers were not affected by the presence of the other. Yet, the luminescence intensity reversibly increased when the spin crossover molecules were switched from the LS to the HS state in the uppermost layer. We found a strict one-to-one correlation between the luminescence modulation (I_{HS}/I_{LS}) and the UV transmittance change with the spin transition (Tr_{HS}/Tr_{LS}). In the same time, neither the spectral shape nor the decay time of the luminescence emission were altered. These results prove that the origin of the luminescence modulation is a direct result of the different attenuation of the exciting UV light in the two spin states. These results also show that luminescence can be a very sensitive indicator of the thermally induced spin transition, which could be exploited for micro- and nanoscale thermal sensing and imaging applications [21,63,64].

Author Contributions: A.-C.B., X.T., L.R. and G.M. carried out sample synthesis and characterization. All authors contributed to the conceptualization, data analysis and writing the paper.

Conflicts of Interest: The authors declare no conflict of interest.

References

1. Amendola, V.; Di Casa, M.; Fabbrizzi, L.; Licchelli, M.; Mangano, C.; Pallavicini, P.; Poggi, A. Mechanical switches of fluorescence. *J. Incl. Phenom. Macrocycl. Chem.* **2001**, *41*, 13–18. [CrossRef]

2. Pischel, U. Molecular switches as platforms for information processing. *Chimia* **2014**, *68*, 505–511. [CrossRef] [PubMed]

3. Cheng, Y.; Jie, W.; Chao, G.; Xin-Ge, L.; Bin, D.; Yan, L. A facile water-stable MOF-based "off-on" fluorescent switch for label-free detection of dopamine in biological fluid. *J. Mater. Chem. B* **2017**, *5*, 2524–2535. [CrossRef]

4. Yang, L.; Jianping, W.; Liang, Y.; Cheng, Z.; Ruilong, Z.; Zhongping, Z.; Bianhua, L.; Changlong, J. Fluorescent paper sensor fabricated by carbazole-based probes for dual visual detection of Cu2+ and gaseous H2S. *RSC Adv.* **2016**, *6*, 5638456391. [CrossRef]

5. Xin, L.; Tao, R.R.; Hong, L.-J.; Cheng, J.; Jiang, Q.; Lu, Y.-M.; Liao, M.-H.; Ye, W.-F.; Lu, N.-N.; Han, F.; et al. Visualizing peroxynitrite fluxes in endothelial cells reveals the dynamic progression of brain vascular injury. *J. Am. Chem. Soc.* **2015**, *137*, 12296–12303.

6. Marc, V.; Benet, M.; Mena, S.; Rabih, O.; Al-Kaysi, J.H.; Guirado, G. Multistimuli-responsive fluorescent switches based on spirocyclic meisenheimer compounds: Smart molecules for the design of optical probes and electrochromic materials. *J. Org. Chem.* **2018**, *83*, 9166–9167.

7. Bao-Hua, D.; Chen, Y.-L. Recent progress in organic mechanoluminescent materials. *Chin. Chem. Lett.* **2018**, *29*, 245–251.

8. Jaume, G.-A.; Swaminathan, S.; Sortino, S.; Raymo, F.M. Plasmonic activation of a fluorescent carbazole-oxazine switch. *Chem. Eur. J.* **2014**, *20*, 10276–10284.

9. Gareau, D.; Desrosiers, A.; Vallee-Belisle, A. Programmable quantitative DNA nanothermometers. *Nano Lett.* **2016**, *16*, 3976–3981. [CrossRef] [PubMed]

10. Bousseksou, A.; Molnar, G.; Salmon, L.; Nicolazzi, N. Molecular spin crossover phenomenon: Recent achievements and prospects. *Chem. Soc. Rev.* **2011**, *40*, 3313–3335. [CrossRef] [PubMed]

11. Garcia, Y.; Gutlich, P. Thermal spin crossover in Mn(II), Mn(III), Cr(II), and Co(III) coordination compounds. *Top. Curr. Chem.* **2004**, *234*, 49–62.

12. Halcrow, M.A. Spin crossover materials. In *Properties and Applications*; Halcrow, M.A., Ed.; John Wiley & Sons Ltd.: Hoboken, NJ, USA, 2013.

13. Bousseksou, A. (Ed.) Spin crossover phenomenon. *C. R. Chim.* **2018**, *12*, 1055–1300.

14. Decurtins, S.; Gütlich, P.; Köhler, C.P.; Spiering, H.; Hauser, A. Light-induced excited spin state trapping in a transition-metal complex: The hexa-1-propyltetrazole-iron (II) tetrafluoroborate spin-crossover system. *Chem. Phys. Lett.* **1984**, *105*, 1–4. [CrossRef]

15. Bousseksou, A.; Boukheddaden, K.; Goiran, M.; Consejo, C.; Boillot, M.L.; Tuchagues, J.P. Dynamic response of the spin-crossover solid Co(H2(fsa)2en)(py)2 to a pulsed magnetic field. *Phys. Rev. B Cover. Condens. Matter. Mater. Phys.* **2002**, *65*. [CrossRef]

16. Kuppusamy, S.K.; Ruben, M. Emerging trends in spin crossover (SCO) based functional materials and devices. *Coord. Chem. Rev.* **2017**, *346*, 176–205.

17. Molnar, G.; Sylvain, R.; Salmon, L.; Nicolazzi, W.; Bousseksou, A. Spin crossover nanomaterials: From fundamental concepts to devices. *Adv. Mater.* **2018**, *30*. [CrossRef]

18. Shepherd, H.; Carlos, J.; Quintero, M.; Molnar, G.; Salmon, L.; Bousseksou, A. *Luminescent Spin-Crossover Materials*; John Wiley & Sons Ltd.: Hoboken, NJ, USA, 2013; pp. 347–373.

19. Marfunin, A.S. *Spectroscopy, Luminescence, and Radiation Centers in Minerals*; Springer: Berlin, Germany, 1979; 352p.

20. Suleimanov, I.; Molnar, G.; Salmon, L.; Bousseksou, A. Near-infrared luminescence switching in a spin-crossover polymer nanocomposite. *Eur. J. Inorg. Chem.* **2017**, 3446–3451. [CrossRef]

21. Salmon, L.; Molnar, G.; Zitouni, D.; Quintero, C.; Bergaud, C.; Micheau, J.-C.; Bousseksou, A. A novel approach for fluorescent thermometry and thermal imaging purposes using spin crossover nanoparticles. *J. Mater. Chem.* **2010**, *20*, 5499–5503. [CrossRef]

22. Piguet, C.; Rivara-Minten, E.; Hopfgartner, G.; Buenzli, J.-C.G. Molecular magnetism and iron(II) spin-state equilibrium as structural probes in heterodinuclear d–f complexes. *Helv. Chim. Acta* **1995**, *78*, 1651–1672. [CrossRef]

23. Wang, C.F.; Li, R.F.; Chen, X.Y.; Wei, R.J.; Zheng, L.S.; Tao, J. Synergetic spin crossover and fluorescence in one-dimensional hybrid complexes. *Angew. Chem. Int. Ed.* **2015**, *54*, 1574–1577. [CrossRef]

24. Lochenie, C.; Wagner, K.G.; Karg, M.; Weber, B. Modulation of the ligand-based fluorescence of 3d metal complexes upon spin state change. *J. Mater. Chem. C* **2015**, *3*, 7925–7935. [CrossRef]

25. Wang, C.F.; Sun, M.J.; Guo, Q.J.; Cao, Z.X.; Zheng, L.S.; Tao, J. Multiple correlations between spin crossover and fluorescence in a dinuclear compound. *Chem. Commun.* **2016**, *52*, 14322–14325. [CrossRef] [PubMed]

26. Estrader, M.; Salinas Uber, J.; Barrios, L.A.; Garcia, J.; Lloyd-Williams, P.; Roubeau, O.; Teat, S.J.; Aromi, G. A magneto-optical molecular device: Interplay of spin crossover, luminescence, photomagnetism, and photochromism. *Angew. Chem. Int. Ed.* **2017**, *56*, 15622–15627. [CrossRef] [PubMed]

27. Kuppusamy Senthil, K.; Salitros, I.; Moreno-Pineda, E.; Ruben, M. Spacer type mediated tunable spin crossover (SCO) characteristics of pyrene decorated 2,6-bis(pyrazol-1-yl)pyridine (bpp) based Fe(II) molecular spintronic modules. *Dalton Trans.* **2017**, *46*, 9765–9768.

28. Schaefer, B.; Bauer, T.; Faus, I.; Wolny, J.A.; Dahms, F.; Fuhr, O.; Lebedkin, S.; Wille, H.-C.; Schlage, K.; Chevalier, K.; et al. A luminescent Pt2Fe spin crossover complex. *Dalton Trans.* **2017**, *46*, 2289–2302. [CrossRef]

29. Wang, J.-L.; Qiang, L.; Yin-Shan, M.; Xin Liu, H.; Zheng, Q.S.; Chun-Ying, D.; Tao, L. Fluorescence modulation via photoinduced spin crossover switched energy transfer from fluorophores to FeII ions. *Chem. Sci.* **2018**, *9*, 2892–2897. [CrossRef]

30. Lochenie, C.; Schoetz, K.; Panzer, F.; Kurz, H.; Maier, B.; Puchtler, F.; Agarwal, S.; Koehler, A.; Weber, B. Spin-crossover iron(II) coordination polymer with fluorescent properties: Correlation between emission properties and spin state. *J. Am. Chem. Soc.* **2018**, *140*, 700–709. [CrossRef]

31. Hasegawa, M.; Franz, R.; Hara, T.; Kikuchi, Y.; Fukuda, Y.; Okubo, J.; Hoshi, T.; Linert, W. Fluorescence spectra of Fe(II) spin crossover complexes with 2,6-bis(benzimidazole-2'-yl)pyridine. *Chem. Phys.* **2002**, *277*, 21–30. [CrossRef]

32. Garcia, Y.; Robert, F.; Naik, A.D.; Zhou, G.; Tinant, B.; Robeyns, K.; Michotte, S.; Piraux, L. Spin transition charted in a fluorophore-tagged thermochromic dinuclear iron(II) complex. *J. Am. Chem. Soc.* **2011**, *133*, 15850–15853. [CrossRef]

33. Gonzalez-Prieto, R.; Fleury, B.; Schramm, F.; Zoppellaro, G.; Chandrasekar, R.; Fuhr, O.; Lebedkin, S.; Kappes, M.; Ruben, M. Tuning the spin-transition properties of pyrene-decorated 2,6-bispyrazolylpyridine based Fe(II) complexes. *Dalton Trans.* **2011**, *40*, 7564–7570. [CrossRef]

34. Santoro, A.; Kershaw Cook, L.J.; Kulmaczewski, R.; Barrett, S.A.; Cespedes, O.; Halcrow, M.A. Iron(II) complexes of tridentate indazolylpyridine ligands: Enhanced spin-crossover hysteresis and ligand-based fluorescence. *Inorg. Chem.* **2015**, *54*, 682–693. [CrossRef]

35. Carine, E.; Piguet, C.; Bunzli, J.-C.G.; Hopfgartner, G. High-spin iron(II) as a semitransparent partner for tuning europium(III) luminescence in heterodimetallic d-f complexes. *Chem. Eur. J.* **2001**, *7*, 3014–3024.

36. Piguet, C.; Rivara-Minten, E.; Bernardinelli, G.; Buenzli, J.-C.G.; Hopfgartner, G. Noncovalent lanthanide podates with predetermined physicochemical properties: Iron(II) spin-state equilibria in self-assembled heterodinuclear d-f supramolecular complexes. *J. Chem. Soc. Dalton Trans.* **1997**, 421–433. [CrossRef]

37. Quintero, C.M.; Gural'skiy, I.A.; Salmon, L.; Molnar, G.; Bergaud, C.; Bousseksou, A. Soft lithographic patterning of spin crossover complexes. Part 1: Fluorescent detection of the spin transition in single nanoobjects. *J. Mater. Chem.* **2012**, *22*, 3745–3751. [CrossRef]

38. Matsuda, M.; Hikaru, I.; Hiroyuki, T. Electroluminescence quenching caused by a spin-crossover transition. *Chem. Lett.* **2008**, *37*, 374–375. [CrossRef]

39. Matsuda, M.; Hikaru, I.; Hiroyuki, T. Reproducible on-off switching of the light emission from the electroluminescent device containing a spin crossover complex. *Thin Solid Films* **2008**, *517*, 1465–1467. [CrossRef]

40. Matsuda, M.; Keita, K.; Ryoma, U.; Nobuaki, K.; Hiroyuki, T. Characteristics of organic light-emitting devices consisting of dye-doped spin crossover complex films. *Thin Solid Films* **2013**, *531*, 451–453. [CrossRef]

41. Gural'skiy, I.A.; Quintero, C.M.; Abdul-Kader, K.; Lopes, M.; Bartual-Murgui, C.; Salmon, L.; Zhao, P.; Molnar, G.; Astruc, D.; Bousseksou, A. Detection of molecular spin-state changes in ultrathin films by photonic methods. *J. Nanophotonics* **2012**, *6*, 63517. [CrossRef]

42. Tovee, C.A.; Kilner, C.A.; Thomas, J.A.; Halcrow, M.A. Co-crystallizing two functional complex molecules in a terpyridine embrace lattice. *Cryst. Eng. Comm.* **2009**, *11*, 2069–2077. [CrossRef]

43. Kershaw Cook, L.J.; Halcrow, M.A. Doping ruthenium complexes into a molecular spin-crossover material. *Polyhedron* **2015**, *87*, 91–97. [CrossRef]

44. Matsukizono, H.; Keita, K.; Nobuo, K. Self-assembly-directed spin conversion of iron(II) 1,2,4-triazole complexes in solution and their effect on photorelaxation processes of fluorescent counter ions. *Chem. Lett.* **2008**, *37*, 446–447. [CrossRef]

45. Titos-Padilla, S.; Herrera, J.M.; Chen, X.-W.; Delgado, J.J.; Colacio, E. Bifunctional Hybrid SiO2 Nanoparticles Showing Synergy between Core Spin Crossover and Shell Luminescence Properties. *Angew. Chem. Int. Ed.* **2011**, *50*, 3290–3293. [CrossRef]

46. Suleimanov, I.; Kraieva, O.; Molnar, G.; Salmon, L.; Bousseksou, A. Enhanced luminescence stability with a Tb-spin crossover nanocomposite for spin state monitoring. *Chem. Commun.* **2015**, *51*, 15098–15101. [CrossRef] [PubMed]

47. Suleimanov, I.; Kraieva, O.; Sanchez Costa, J.; Fritsky, I.O.; Molnar, G.; Salmon, L.; Bousseksou, A. Electronic communication between fluorescent pyrene excimers and spin crossover complexes in nanocomposite particles. *J. Mater. Chem. C* **2015**, *3*, 5026–5032. [CrossRef]

48. Kraieva, O.; Suleimanov, I.; Molnar, G.; Salmon, L.; Bousseksou, A. CdTe quantum dot fluorescence modulation by spin crossover. *Magnetochemistry* **2016**, *2*, 11. [CrossRef]

49. Luo, Y.-H.; Jing-Wen, W.; Wen, W.; Xiao-Tong, H.; Dan-Li, H.; Chen Chen, T.X.; Qiyue, S.; Bai-Wang, S. Bidirectional photoswitching via alternating NIR and UV irradiation on a core-shell UCNP-SCO nanosphere. *ACS Appl. Mater. Interfaces* **2018**, *10*, 16666–16673. [CrossRef]

50. Herrera, J.M.; Titos-Padilla, S.; Pope, S.J.A.; Berlanga, I.; Zamora, F.; Delgado, J.J.; Kamenev, K.V.; Wang, X.; Prescimone, A.; Brechin, E.K.; et al. Studies on bifunctional Fe(II)-triazole spin crossover nanoparticles: Time-dependent luminescence, surface grafting and the effect of a silica shell and hydrostatic pressure on the magnetic properties. *J. Mater. Chem. C* **2015**, *3*, 7819–7829. [CrossRef]

51. Rat, S.; Ridier, K.; Vendier, L.; Molnar, G.; Salmon, L.; Bousseksou, A. Solvatomorphism and structural-spin crossover property relationship in bis[hydrotris(1,2,4-triazol-1-yl)borate]iron(II). *Cryst. Eng. Comm.* **2017**, *19*, 3271–3280. [CrossRef]

52. Shalabaeva, V.; Mikolasek, M.; Manrique-Juarez, M.D.; Bas, A.-C.; Rat, S.; Salmon, L.; Nicolazzi, W.; Molnar, G.; Bousseksou, A. Unprecedented size effect on the phase stability of molecular thin films displaying a spin transition. *J. Phys. Chem. C* **2017**, *121*, 25617–25621. [CrossRef]

53. Shalabaeva, V.; Rat, S.; Manrique-Juarez, M.D.; Bas, A.-C.; Vendier, L.; Salmon, L.; Molnar, G.; Bousseksou, A. Vacuum deposition of high-quality thin films displaying spin transition near room temperature. *J. Mater. Chem. C* **2017**, *5*, 4419–4425. [CrossRef]

54. Manrique-Juarez, M.D.; Mathieu, F.; Shalabaeva, V.; Cacheux, J.; Rat, S.; Nicu, L.; Leichle, T.; Salmon, L.; Molnar, G.; Bousseksou, A. A bistable microelectromechanical system actuated by spin-crossover molecules. *Angew. Chem. Int. Ed.* **2017**, *56*, 8074–8078. [CrossRef]

55. Ridier, K.; Rat, S.; Salmon, L.; Nicolazzi, W.; Molnar, G.; Bousseksou, A. Scan-rate and vacuum pressure dependence of the nucleation and growth dynamics in a spin-crossover single crystal: The role of latent heat. *Phys. Chem. Chem. Phys.* **2018**, *20*, 913–945. [CrossRef]

56. Shalabaeva, V.; Ridier, K.; Rat, S.; Manrique-Juarez, M.D.; Salmon, L.; Seguy, I.; Rotaru, A.; Molnar, G.; Bousseksou, A. Room temperature current modulation in large area electronic junctions of spin crossover thin films. *Appl. Phys. Lett.* **2018**, *112*. [CrossRef]

57. Mikolasek, M.; Manrique-Juarez, M.D.; Shepherd, H.J.; Ridier, K.; Rat, S.; Shalabaeva, V.; Bas, A.-C.; Collings, I.E.; Mathieu, F.; Cacheux, J.; et al. Complete set of elastic moduli of a spin-crossover solid: Spin-state dependence and mechanical actuation. *J. Am. Chem. Soc.* **2018**, *140*, 8970–8979. [CrossRef]

58. Ridier, K.; Rat, S.; Shepherd, H.J.; Salmon, L.; Nicolazzi, W.; Molnar, G.; Bousseksou, A. Spatiotemporal dynamics of the spin transition in [Fe(HB(tz)3)2] single crystals. *Phys. Rev. B* **2017**, *96*, 134106. [CrossRef]

59. Adachi, C.; Baldo, M.A.; Forrest, S.R.; Thompson, M.E. High-efficiency organic electrophosphorescent devices with tris(2-phenylpyridine)iridium doped into electron-transporting materials. *Appl. Phys. Lett.* **2000**, *77*, 904–906. [CrossRef]

60. Kawamura, Y.; Brooks, J.; Brown, J.J.; Sasabe, H.; Adachi, C. Intermolecular interaction and a concentration-quenching mechanism of phosphorescent Ir(III) complexes in a solid film. *Phys. Rev. Lett.* **2006**, *96*, 017404. [CrossRef]

61. Taiju, T.; Aljaroudi, N. Energy transfer between Ir(ppy)3 molecules in neat film and concentration quenching of phosphorescence. *Opt. Mater.* **2008**, *30*, 1375–1381.

62. Namdas, E.B.; Ruseckas, A.; Samuel, I.D.W.; Lo, S.-C.; Burn, P.L. Photophysics of Fac-Tris(2-Phenylpyridine) iridium(III) cored electroluminescent dendrimers in Solution and films. *J. Phys. Chem. B* **2004**, *108*, 1570–1577. [CrossRef]

63. Low, P.; Kim, B.; Takama, N.; Bergaud, C. High-spatial-resolution surface-temperature mapping using fluorescent thermometry. *Small* **2008**, *4*, 908–914. [CrossRef]

64. Vetrone, F.; Naccache, R.; Zamarron, A.; Juarranz de la Fuente, A.; Sanz-Rodriguez, F.; Martinez Maestro, L.; Martin Rodriguez, E.; Jaque, D.; Sole, H.G.; Capobianco, J.A. Temperature Sensing Using Fluorescent Nanothermometers. *ACS Nano* **2010**, *4*, 3254–3258. [CrossRef] [PubMed]